IEEE Access
Multidisciplinary | Rapid Review | Open Access Journal

Received January 28, 2019, accepted February 18, 2019, date of publication February 27, 2019, date of current version March 20, 2019.

*Digital Object Identifier 10.1109/ACCESS.2019.2902104*

# Communication Aspects for a Measurement Based UWB In-Body to On-Body Channel

**PÅL ANDERS FLOOR[1], RAÚL CHÁVEZ-SANTIAGO[2,3], ANNA N. KIM[4], KIMMO KANSANEN[5], TOR A. RAMSTAD[5], AND ILANGKO BALASINGHAM[2,4], (Senior Member, IEEE)**

[1]Department of Computer Science, Norwegian University of Science and Technology, NO-2802 Gjøvik, Norway
[2]Intervention Center, Oslo University Hospital, N-0027 Oslo, Norway
[3]BodyComm Technologies LLC, Oaxaca, Mexico
[4]Elliptic Laboratories, 0180 Oslo, Norway
[5]Department of Electronic Systems, Norwegian University of Science and Technology, NO-7491 Trondheim, Norway

Corresponding author: Pål Anders Floor (paal.anders.floor@ntnu.no)

This work was supported by the Research Council of Norway through the project Medical Sensing, Localization, and Communication using Ultra Wideband Technology Phase II (MELODY II) under Grant 225885.

**ABSTRACT** A wireless capsule endoscopy (WCE) is a good option for the screening of the digestive system. To better facilitate detection of diseases at an early stage, gastroenterologists seek both higher frame rate and frame resolution than what is offered in the current WCE standards. This necessitates higher data rate links through the human body. One possible way to obtain a high data rate without significantly increasing the transmission power is to use a large bandwidth, making ultra-wideband communication (UWB) a good candidate. However, in order to properly utilize the large bandwidth available through UWB communication, it is important that the channel attenuation does not increase too rapidly with frequency. In this paper, we investigate obtainable rates and necessary transmission power for an in-body to on-body UWB channel model in the 1-6 GHz range based on measurements taken in the abdominal region of several porcine subjects. We consider both the theoretically attainable minimum power needed to obtain a given capacity and the power needed to obtain the same rate with practically implementable modulation- and coding schemes for a target bit error rate. The presented results show that huge savings in transmission power are possible by communicating in the lower frequency ranges ($1 - 2$ GHz) where the attenuation is less severe. Further, about a 10-fold increase in transmission power has to be expected when practically implementable schemes are considered compared with the minimum achievable power derived from a capacity perspective. It is also illustrated that little is gained in terms of lowered power consumption (or increased rates) by using a bandwidth larger than 1 GHz due to the rate of decline of the channels transfer function with frequency.

**INDEX TERMS** In-body to on-body communication, ultra-wideband, transmission power, capacity, modulation, channel coding.

## I. INTRODUCTION

Severe diseases in the digestive system like Chrons disease, inflammatory bowel disease, as well as several types of cancers, are becoming more and more common. One way to detect such diseases at an early stage, thereby making them more likely to combat, is to make screening of the digestive system a common procedure beyond a certain age, suggested by some as early as 45 years [1]. In order to motivate as many people as possible to perform such a screening, it is vital that the procedure is not too unpleasant, adequately safe and relatively cheap. This may rule out many common screening methods, for example the endoscope and gastroscope, which are uncomfortable and not capable of reaching parts of the small bowel without inflicting severe pain to the patient.

The *wireless capsule endoscope* (WCE) [2], [3], which is a pill-sized capsule (typically of size 11 mm x 32 mm, weighing less than 4 grams) that the patient swallows, is a good alternative for screening. The WCE carries one- or several cameras on board recording video of the gastrointestinal system while travelling through it, and is capable of reaching all parts of the digestive system.

One of the main drawbacks with the current standard WCEs is that the video quality is significantly lower than that provided by gastroscopy and endoscopy [2], [3]. For the gastroenterologist to detect all features of interest, especially in parts of the digestive system where the WCE moves relatively fast (like the esophagus and parts of the colon), it is necessary

The associate editor coordinating the review of this manuscript and approving it for publication was Ke Guan.

to increase both the number of images taken per second (the *frame-rate*) as well as the resolution of each image taken. This necessitates lager streams of data to be transmitted which again requires a significantly higher data-rate than that provided by current WCEs. This increase in transmission rate should be obtained without placing significantly harder demands on battery power, as the battery is already pushed to the limit in current WCEs [3]. For medical reasons it is also important to keep the power radiated into the human body as low as possible.

One possible way of obtaining a higher data rate without increasing the transmission power is to use a large channel bandwidth [4, p. 273], making *Ultra Wide Band* (UWB) communication a natural choice [5].[1] However, to properly utilize UWB, the relevant channel has to have certain characteristics, like a slow enough decay of the transfer function's magnitude with frequency. If the channels transfer function decays too rapidly, UWB will provide little- or no benefit over narrowband alternatives, like communication in the *Medical Implant Communication Service* (MICS) band [6] (402-405 MHz and 2360-2400 MHz bands). Can UWB communication provide a significant benefit for a typical *in-body to on-body* (IB-to-OB)[2] abdominal channel over narrowband communication in terms of increased rates and low power consumption?

Several efforts have dealt with UWB for WCE. In [7], Brumm and Bauch determine the channel capacity for the IB-to-OB channel for a simplified multi-layered channel model, developed by the same authors, over the non licensed band $3.1 - 10.6$ GHz. Their results show that multiple receiver antennas, placed in certain configurations on the body, are necessary in order to improve over the MICS band. However, as the authors also show, larger attenuation has to be expected in a real IB-to-OB channel, where one example is the measurement based path loss model we apply in this paper (see [7, Fig. 7]). Further, the same authors show in [8] that capacity does not increase significantly by increasing the bandwidth beyond 1 GHz. In [9] the bit error rate (BER) performance with diversity reception for the IB-to-OB UWB channel in the 3.4 - 4.8 GHz range was quantified. In [10], an IB-antenna for transmitter diversity was tested on a living animal subject. In [11], Katsu et. al. performed an experimental evaluation of correlation and energy detection for 3.4 - 4.8 GHz UWB channel using *Multi-Pulse Position Modulation* and showed that for a path loss of 75 dB, a rate of 2 Mbps can be obtained with a BER of $10^{-2}$.

The main objective of this paper is to determine the necessary transmission power needed to obtain certain datarates for a 1-6 GHz UWB IB-to-OB channel obtained from measurements in the abdominal region on living porcine subjects [12]. Although parts of this band is licensed, exceptions may be possible, especially in a hospital environment, if proper measures are taken, like adequate shielding. We first present the relevant path loss model and evaluate its *coherence bandwidth*. We then evaluate the necessary transmission power for several scenarios. First we investigate how the minimum obtainable transmit power for a given capacity constraint is affected by frequency band selection as well as the relevant bandwidth used. We then evaluate how much one must increase the power as practically implementable schemes are considered. Since UWB is assumed, *Pulse Position Modulation* (PPM) is a natural choice as it is known to be well performing at very low transmission power when a large channel bandwidth is available [13, pp. 666-674].[3] However, since we emphasize high data rate, Quadrature Phase Shift Keying (QPSK) is also evaluated. First we compare the relevant modulation schemes using capacity achieving channel codes, that is, the capacity of the channel with modulated input. Then we investigate both uncoded modulation as well as coded modulation. We apply *Reed-Solomon* (RS) codes [14] since they operate directly on multilevel symbols, and are efficient at correcting error bursts that are common for IB-to-OB channels. The results presented may also apply as guidelines on how to choose frequency ranges, modulation cardinality as well as channel code block length for UWB IB-to-OB channels. To assess the benefits of UWB over narrowband communication we also compare our results to the 402-405 MHz MICS band, using the path loss model derived in [15].

Although we emphasised on WCE above, the analysis provided in this paper is not limited to WCE applications, but can be used for any potential in-body device. However, the WCE is one important example where a high datarate channel through the human body is needed.

The paper is organized as follows: In section II the problem definition is given. In Section III the relevant IB-to-OB channel is presented, its coherence bandwidth is investigated and the capacity as well as the necessary power needed to achieve a specified rate are calculated. In Section IV we investigate necessary transmission power needed for implementable modulation and coding schemes for the relevant channel model. Finally, a summary as well as conclusions are given in Section V.

## II. PROBLEM DEFINITION AND ASSUMPTIONS

Fig. 1(a) depicts a typical WCE communication system. We will concentrate on the channel coder, modulator and wireless channel in this paper. We focus on the wireless UWB IB-to-OB communication link depicted in Fig. 1(b) in the first part of the paper, corresponding to the content of the ''Wireless IB-to-OB Channel'' and ''Demodulation & detection'' blocks in Fig. 1(a). We provide more details on the coding and modulation part in Section IV.

The UWB communication is assumed to be pulse-based (see Section IV). The output from the encoder to the IB-to-OB

[1] UWB signals are those with fractional bandwidth exceeding 20% of the center frequency, or a bandwidth $> 500$ MHz.

[2] We use the abbreviation IB for ''in-body'', OB for ''on-body'', and IB-to-OB for ''in-body to on-body'' throughout the paper.

[3] Note that this is a somewhat different scheme than the MPPM scheme in [11] where each source bit is represented as a set of pulse positions. The PPM considered here represent several bits in one single pulse.

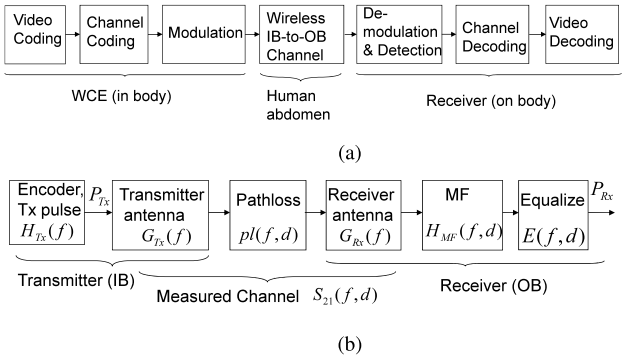


**FIGURE 1. (a) Typical WCE communication system. (b) Block diagram for wireless UWB IB-to-OB communication link, corresponding to the "Wireless IB-to-OB Channel" and "Demodulation & detection" blocks in Fig. 1(a).**

channel is then represented by pulses with frequency response $H_{Tx}(f)$.

The transmitter and receiver antenna responses (or gains) are $G_{Tx}$ and $G_{Rx}$, respectively. Since the orientation of the WCE continually changes, the ideal transmitter antenna should be isotropic. However, this is not possible in practice. We discuss antennas further in Section III-A1. The channel attenuation, including loss due to the inverse square law, is incorporated into $pl(f, d)$, being a function of both frequency and depth. At the receiver a *matched filter* (MF) detector, $H_{MF}(f, d)$, is assumed. The MF can be matched to either the transmitter pulse, $H_{Tx}(f)$, or both the transmitter pulse as well as the channel (including the antenna responses), depending on the availability of channel state information (CSI). If perfect *channel state information* (CSI) cannot be obtained, an equalizer may be needed in order to reduce the effect of multi-path reflections, especially at larger depths, $d$. $P_{Tx}$ and $P_{Rx}$ denote the transmitter and receiver power, respectively. The link budget can be formulated based on the well-known Friis transmission formula [16]. A simplified model was presented in [17]. However, to incorporate the frequency selectivity that follows with the large bandwidth of UWB systems, the Friis formula has to be extended to transfer functions.

The path loss model applied in this paper, $PL(f, d)$, is based on measurements where several of the blocks in Fig. 1(b) are measured as one response (see Section III-A). The model includes transmitter antenna, the channel path loss as well as the receiver antenna, denoted $S_{21}(f, d)$ in Fig. 1(b). We will assume an ideal MF matched to both the Tx-pulse, $H_{Tx}$, as well as the measured channel response, $S_{21}$. The equalizer can therefore be omitted in the rest of the paper. With

$$H_{\mathrm{Rx}}(f, d) = H_{Tx}(f)S_{21}(f, d), \tag{1}$$

the MF is given by

$$H_{\mathrm{MF}}(f, d) = KH^{*}_{\mathrm{Rx}}(f, d)e^{-j2\pi fT}, \tag{2}$$

where the exponential is a phase term that depends on the path delay $T$, and $K$ is a normalization factor (see for example [18]). Since $K$ scales both the received signal and the noise, it will cancel out in the signal-to-noise ratio. We therefore choose $K = 1$ without loss of generality. The ratio between received and transmitted power will be useful throughout the paper and is given by

$$\begin{aligned}\gamma(d) = \frac{P_{Rx}}{P_{Tx}} &= \int_{f_l}^{f_h} |H_{\mathrm{Rx}}(f, d)|^2 \mathrm{d}f \\ &= \int_{f_l}^{f_h} |H_{Tx}(f)S_{21}(f, d)|^2 \mathrm{d}f,\end{aligned} \tag{3}$$

where $f_l$ and $f_h$ are the lower and upper frequencies of the relevant frequency band respectively.

We also assume perfect synchronization and timing between transmitter and receiver throughout the paper.

## III. PATH LOSS MODEL, COHERENCE BANDWIDTH AND CAPACITY

In this section we present the path loss model for IB-to-OB communication and calculate the coherence bandwidth as well as its capacity.

### A. PATH LOSS MODEL

The path loss model applied throughout the paper is based on scattering matrix (S) measurements taken in the abdominal region on anesthetized porcine subjects in three separate experiments performed at Oslo University Hospital [10], [12].

#### 1) NOTES ON EXPERIMENT AND ANTENNAS

The details of the measurement procedure as well as all equipment being used are provided in [12] and [10]. We summarize information important for the current paper here.

In all three experiments different porcine subjects were applied. In the first and second experiments the same set of transmitter-and receiver antennas was applied, whereas in the third experiment a different set of antennas was applied.

Both transmitter antennas had shape and size making them suitable for a typical WCE and both had a quasi omnidirectional radiation pattern (for details see [12], [19] for experiments 1 and 2, and [10] for experiment 3). The receiver antennas were both dipoles (for details see [20] for experiments 1 and 2, and [10] for experiment 3). Constructing an on-body receiver antenna covering the whole $1-6$ GHz range is relatively straight forward as size is not an issue. However, constructing an in-body miniature-sized transmitter antenna having a relatively flat response over the $1-6$ GHz range is not easy. In that case, one have to choose a certain frequency band, then optimize the antenna for that band. During a measurement procedure, there is not enough time to test several transmitter antennas, as obtaining enough measurement points require most of the available time. It was therefore chosen to use available antennas optimized for the non-licensed band $3.1-4.8$ GHz (lying around the middle to upper end

of the relevant frequency band). The obtained results are therefore pessimistic in the lower frequency ranges.

To obtain a more realistic response that will be closer to what can be expected in practical propagation situations, one can compensate for the return loss over the transmitter antennas non-optimal frequency ranges by using the $S_{11}$ response (reflection factor) which was measured during the experiments. This compensation has been done for all data provided in this paper using the method in [12], Eq. (2).

Compensation for non-optimal radiation pattern, on the other hand, is not possible. Therefore improvements in performance, especially in the lower frequency ranges, can be expected with an antenna optimized in that range, as it would improve the gain $G_{Tx}$ in Fig. 1(b).

With a different set of antennas, one can use the same approach as provided in this paper to obtain similar results by simply replacing the $S_{21}(f, d)$ response in (1) by any new measured response.

### 2) DERIVATION AND CHARACTERISTICS OF PATH LOSS MODEL

As only two out of the three experiments were conducted before the path loss model in [12] was derived, we need to re-derive the model here with data from the third experiment included.

A path loss formula as a function of the propagation distance, $d$, and frequency, $f$, is obtained by fitting exponential curves to the data provided from all the transfer function measurements obtained in the three experiments. That is, we fit data to $|S_{21}|$, where $S_{21}$ is the average forward transfer function obtained by averaging all measurement trials conducted for each of the measurement points in [12] and [10]. The well-known log-distance model for in-body channels given in [6] was applied

$$PL(d,f) = PL_0 + 10N(f)\log_{10}\left(\frac{d}{d_0}\right), \tag{4}$$

where $d$ is the separation between antennas (i.e., implantation depth in centimeters) and $d_0$ is the reference implantation depth with a value of 4.5 cm (the most shallow depth for which it was possible to obtain reliable measurements). $PL_0$ is the path loss measured at reference depth $d_0 = 4.5$ cm. The path loss exponent, $N(f)$, was found by a non-linear least squares curve fitting algorithm. Fig. 2 shows scatter plots for all obtained measurements as well as the curve fitting of (4) for 2 GHz and 4 GHz, respectively. The spread shown in Fig. 2 around the fitted line is due to scattering from different organs and tissues with different dielectric properties that affects the electromagnetic wave propagation. For the WCE this will lead to "shadowing". We illustrate the effect this spread has on the transmission power needed to obtain a certain data rate (or capacity) in Section III-C. One important observation is that although different porcine subjects as well as transmitter- and receiver antennas were applied in the three experiments, the channel responses follow more or less the same trend. It is therefore likely that the model is not too far away from what one can expect in a practical situation.

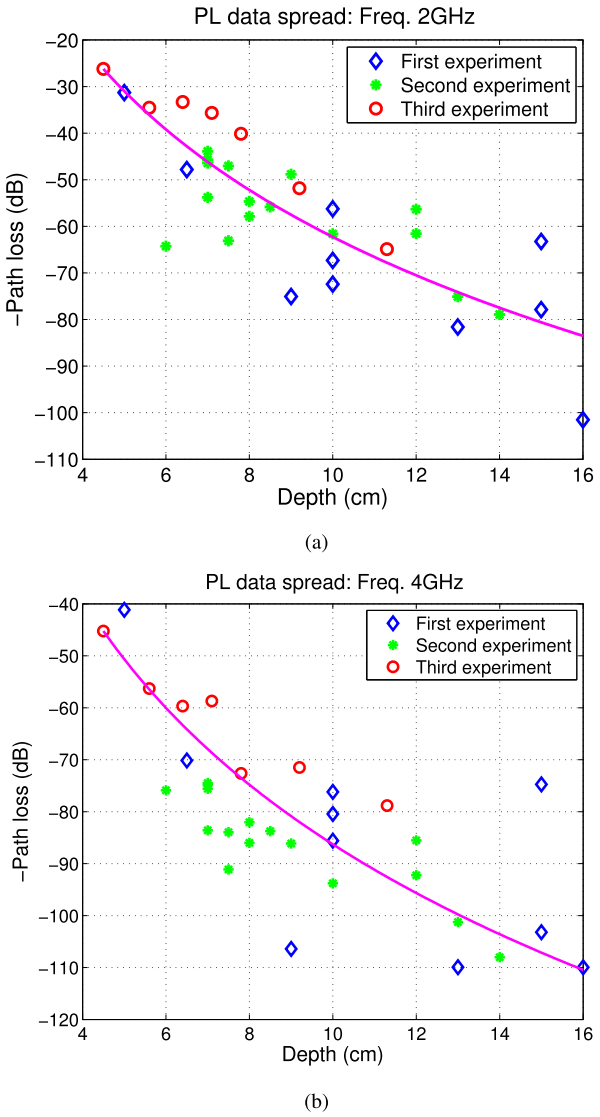


**FIGURE 2.** Curvefitting to experiment data. (a) 2GHz. (b) 4GHz.

Due to the frequency dependency of dielectric properties of the different organs and tissues, the rate at which the path loss increases with distance is a function of frequency, $f$. This rate is expressed by the path loss exponent denoted as $N(f)$. In [12] $N(f)$ was shown to closely follow a 2nd degree polynomial. However, when results from the third experiment were added, $N(f)$ was better fitted to a 6th degree polynomial $N(f) = c_6 f^6 + c_5 f^5 + c_4 f^4 + c_3 f^3 + c_2 + f^2\, c_1 f + c_0$, with coefficients $c_6 = -0.019618$, $c_5 = 0.39352$, $c_4 = -3.0217$, $c_3 = 11.302$, $c_2 = 22.969$, $c_1 = 29.22$ and $c_0 = -10.426$. Note that these coefficients are fitted to data for depths between 4.5-16 cm. Hence, the behavior of the presented model outside this range can be different. By inserting the above polynomial into (4) and using the $|S_{21}|$ data obtained at depth $d_0 = 4.5$ cm for $PL_0$, the two-dimensional path loss

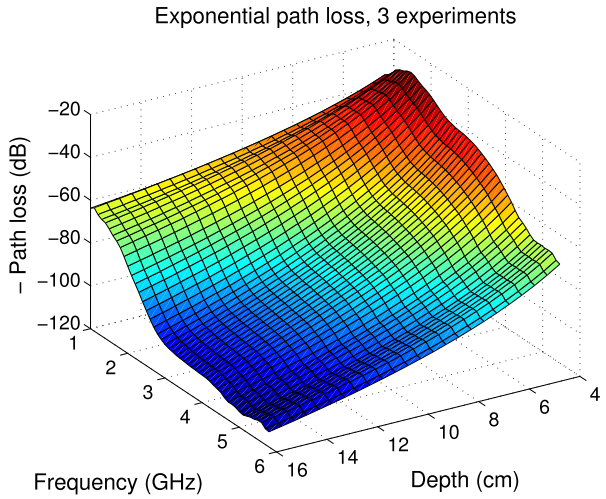


**FIGURE 3.** Average path loss as function of frequency and depth.

profile in Fig. 3 as a function of both frequency and depth was obtained.

From the graphics in Fig. 3 it is clear that the wave propagation at lower frequencies (i.e., within 1-3 GHz range) exhibits significantly lower path loss. We shall see in Section III-C that the lower frequency ranges are beneficial also from a capacity perspective. The slight decline in the PL function at the lowest frequencies is likely caused by the transmitter antenna being sub-optimal in that range [19].

### B. COHERENCE BANDWIDTH

The frequency band where one can expect a wireless channel to be "flat", that is, where the channel treats frequency components of the transmitted signal equally, is the *coherence bandwidth* (CBW). The measurements in [12] and [10] showed that the frequency selectivity of the IB-to-OB channel changed from one measurement point to the other, mostly so for different depths. For a moving device, like the WCE, it is therefore convenient to consider CBW. The CBW is of particular interest when power allocation is not implemented, as it indicates which bandwidth is most useful.

The CBW can be determined from the autocorrelation function (ACF) of the transfer function, $R_H(\Omega) = E\{H(f + \Omega)H^*(f)\}$, named "frequency correlation function" [21, p. 188]. The CBW is defined as the lowest value of $\Omega$ where the ACF, $R_H(\Omega)$, takes on a fixed value. This fixed value is the "correlation", which we denote $\rho$. The CBW is typically taken to be the smallest value of $\Omega$ corresponding to $\rho = 0.5$ or 0.9 [21, p. 188].

Generally, a IB-to-OB channel has a *time-variant transfer function* $H(f, t)$, leading to a time variant frequency correlation function. However, measurement results presented in [12] show that the channel's frequency response at a fixed measurement point (that is, both transmitter and receiver are fixed) varied little from trial to trial, implying that the channel frequency response stays approximately constant at

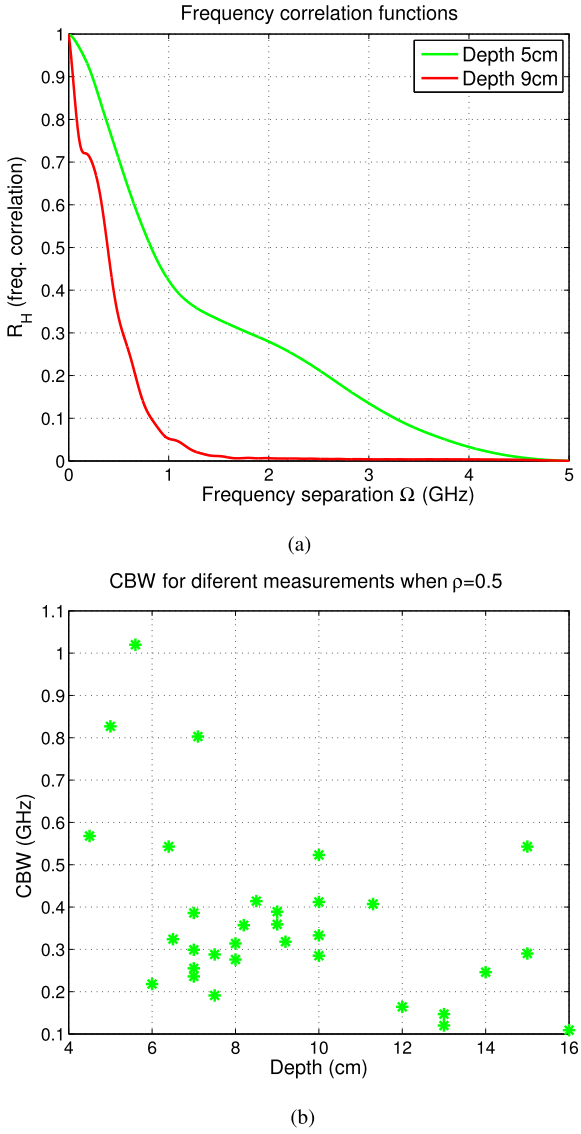


**FIGURE 4.** CBW estimated from experimental data over the whole 1-6 GHz range. (a) Example on frequency correlation functions. (b) Spread in CBW for different measurement points when $\rho = 0.5$.

a fixed point over time. That is, for a given fixed depth at a specific measurement point, $H(f, t) \approx H(f)$, over a relatively long time window. Therefore we can compute the channel's frequency correlation function as $R_H(\Omega) = E\{H(f + \Omega)H^*(f)\}$ for each fixed measurement point as a good approximation.

Fig. 4(a) shows examples of the frequency correlation function at two different depths, $d = 5$ and 9 cm. In Fig. 4(a), the range of $R_H$ is on the vertical axis, while "frequency separation" $\Omega$, that is the CBW for a given $\rho$, are on the horizontal axis. In general, the trend is that the correlation function narrows at larger depths. This is expected as the channel will be affected largely by scattering due to additional layers of tissue at larger depths, and is therefore highly frequency selective (implying a smaller CBW). Fig. 4(b) depicts the CBW calculated at the correlation value $\rho = 0.5$ for all

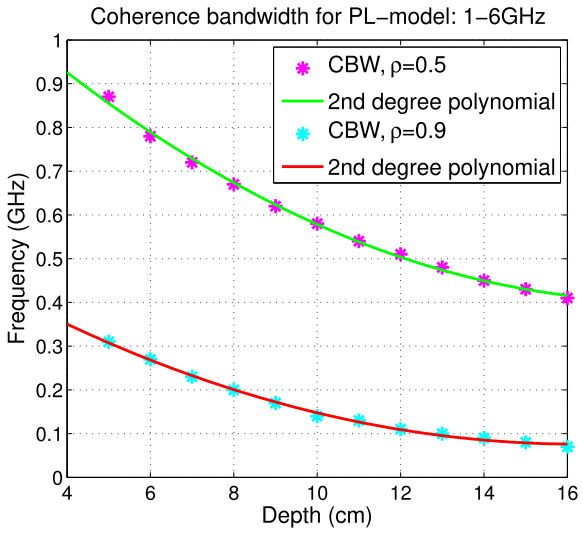


(a)

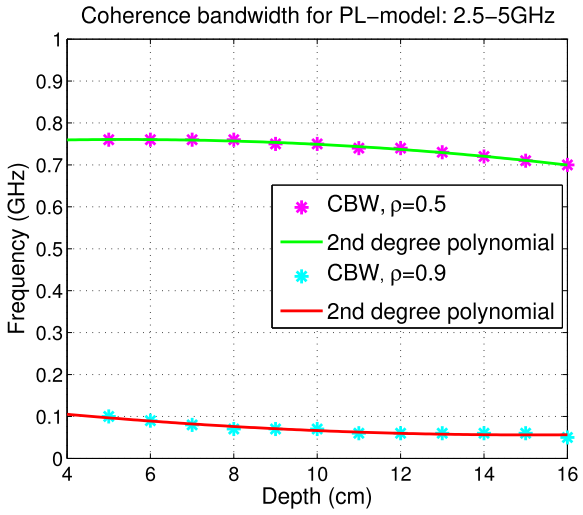


(b)

**FIGURE 5.** CBW for the PL-model in Fig. 3 for $\rho = 0.5$ and 0.9 in: (a) 1 – 6 GHz range. (b) 2.5 – 5 GHz range.

responses corresponding to the different measurement points depicted in Fig. 2. CBW is along the vertical axis wile depth is along the horizontal axis. It shows that the measured channel responses can be seen as approximately flat up to a bandwidth of at most 0.5 GHz for depths larger than 6cm. For shallower depths the CBW increases somewhat.

Although the CBW clearly decays with depth, there is a relatively large spread in the CBW for a given depth, as seen in Fig. 4(b). One possible way of determining a representative value of the CBW for a given depth is to calculate its average over all measurements obtained for that depth. We use the CBW calculated from the path loss model presented in Section III-A as an example throughout the rest of the paper. Fig. 5(a) shows the CBW for the path loss model in Fig. 3 for $\rho = 0.5$ and 0.9 in the whole $1 - 6$ GHz band. By following the same procedure for the $2.5 - 5$ GHz band, one obtains the curves in Fig. 5(b). Clearly, there is a smaller decay in CBW with depth in the higher frequency range, i.e., the $\rho = 0.5$ CBW stays between $700 - 800$ MHz. The reason may be that the PL model is getting somewhat "flatter" in the $2.5-5$ GHz frequency ranges as can be observed in Fig. 3.

Note that since implants are more or less fixed, and typical moving objects, like the WCE, move relatively slowly on average, the channel will also be slowly varying. Therefore the above results gives an indication on the CBW for such applications. The CBW profile seen in Fig. 5(a) is not too far away from that obtained in the lower frequency ranges $(1 - 3$ GHz). We will therefore use this profile when determining the CBW later in this paper.

### C. CAPACITY FOR IB-TO-OB CHANNEL

We want to determine the maximum data rate one can transmit for a given power constraint, or the minimum transmission power needed for a given capacity constraint for the path loss model presented in Section III-A.

For a given frequency response, $H(f)$, the capacity can be calculated from the formula [22, pp. 183-185]

$$C = \int_{f_l}^{f_h} \log_2 \left(1 + \frac{P^*(f)|H(f)|^2}{N_0}\right) \mathrm{d}f, \tag{5}$$

where $f_l$ and $f_h$ are the minimum and maximum frequency, respectively. $P^*(f)$ is the optimally allocated (symbol) power given by

$$P^*(f) = \left(\frac{1}{\lambda} - \frac{N_0}{|H(f)|^2}\right)^+, \tag{6}$$

where $\lambda$ is a Lagrange multiplier and $N_0 = k_B T_e$ is the noise power spectral density. $k_B$ is Boltzmanns constant and $T_e$ the equivalent noise temperature of the receiver (in Kelvin). $(\cdot)^+$ means that only positive values are included. The Lagrange multiplier $\lambda$ (or the *waterfilling level* $1/\lambda$) has to be chosen so that

$$\int_{f_l}^{f_h} P^*(f)\mathrm{d}f = P_{T_{\max}}, \tag{7}$$

where $P_{T_{\max}}$ is the maximum allowed average transmitter (symbol) power. These formulas imply that for a given constraint, $P_{T_{\max}}$, any parts of the spectrum where $N_0/|H(f)|^2 > 1/\lambda$ should not be used (as these will be under the noise floor) and that most power should be allocated to the "deepest valleys" of $N_0/|H(f)|^2$, corresponding to the frequencies where the attenuation is smallest. One can also apply these equations for the same spectra to determine the minimum transmission power needed for a given capacity constraint.

As discussed in Section III-B, the IB-to-OB channel has slowly varying dynamics. Therefore, the formula in (5) applies to the PL-model in Section III-A if we assume the ideal situation where noise is added by the receiver equipment only. This can approximately be obtained by proper shielding of the receiver from the surrounding environment, since little or no electromagnetic radiation will reach inside the body

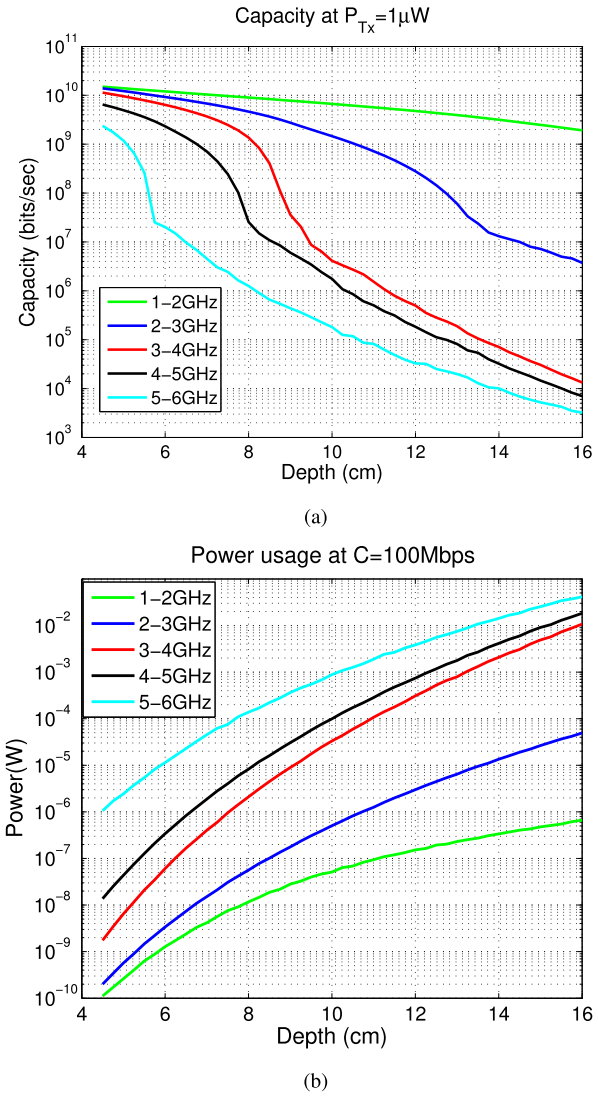


**FIGURE 6.** (a) Capacity at 1 $\mu$W power constraint as a function of depth (b) Necessary transmit power at 100 Mbps capacity constraint with 1 GHz bandwidth as a function of depth.

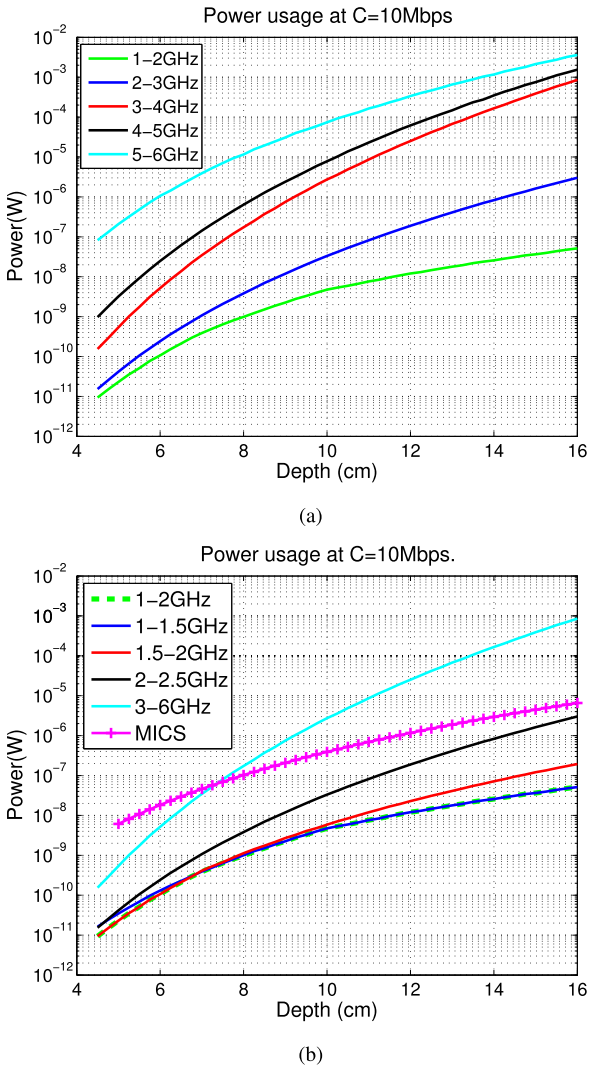


**FIGURE 7.** Necessary transmit power at 10 Mbps capacity constraint. (a) Bandwidth 1 GHz. (b) Varying bandwidth as well as the 402-405 MHz MICS band.

due to the large attenuation there. To compute the average capacity as a function of depth, one can insert the path loss model in (4) through

$$H(f, d) = 10^{PL(d,f)/10}, \tag{8}$$

then substitute the obtained response, $H(f, d)$, into equations (5)-(7). Capacity is then dependent on both frequency and depth.

Fig. 6(a) shows the average capacity as a function of depth for different frequency ranges with 1 GHz bandwidth, transmitter power constraint $P_{T_{\max}} = 1\mu$W, and $T_e = 293$ K (room temperature in Kelvin) and Fig. 6(b) shows the necessary power for a rate constraint of 100 Mbps and 1 GHz bandwidth. From Fig. 6(a) one can observe a change in the slopes of the capacity as depth increases, most significantly so in the higher frequency ranges. One likely reason is that more and more of the frequency spectrum becomes useless as the depth increases due to high attenuation. Therefore the power is allocated to narrower frequency bands. This is in line with the CBW investigation in Section III-B. Fig. 7 shows the necessary power for a capacity constraint of 10 Mbps for different frequency ranges and different bandwidths. We also include the minimal power usage obtained using the $402 - 405$ MHz MICS band for the 10 Mbps constraint (100 Mbps cannot be supported by such a small bandwidth at a reasonable low level of transmission power). The curve was obtained by using the path loss model in [15] assuming a flat response over the whole $402 - 405$ MHz band, then applying the well-known capacity formula for a bandlimited Gaussian channel [4, p.273] with transmitter and receiver power related through a fixed attenuation factor determined by the relevant path loss model.

It is clear from these plots that it is advantageous to use the lower frequency ranges: From Fig. 7(b) one can observe that even when the whole range between 3-6 GHz is applied, it requires a much higher transmission power compared to the lower frequency ranges, even for a bandwidth of only

500 MHz. For frequencies in the range 3-6 GHz (and above) one have to use at least 1 mW of power on average for depths deeper than 16 cm to achieve a rate of 10 Mbps, and at least 10 mW of power on average to achieve a rate of 100 Mbps, compared to approximately 50 nW and 0.5 $\mu$W in the 1-2 GHz band, respectively. That is, a factor of about $2 \cdot 10^4$. Also note that little power is saved at larger depths by increasing bandwidth beyond 1 GHz. The reason is that the spectrum declines significantly over a bandwidth of 1 GHz, mostly so at larger depths. This is also indicated by the CBW shown in Figs. 4(b) and 5 and is in line with the investigations in [8]. Also note that to obtain benefits over the MICS band for a capacity of 10 Mbps at larger depths, one should chose a frequency band below 2.5 GHz.

To get a fair idea of the necessary transmission power needed to obtain a certain capacity at each measurement point depicted in Fig. 2, and thereby the spread around the average transmission power, one can compute the average $|S_{21}|$ response over all measurement trials and insert the result $H(f) = |S_{21}|$ in equations (5)-(7), then (numerically) solve w.r.t. $P_{T_{\max}}$. Fig. 2 shows that a large spread around the average model must be accounted for. How this spread affects the minimum power required for a given rate constraint compared to the PL-model is shown in Fig. 8 for the frequency bands 1-2 GHz and 3-4 GHz. Note that the PL-model gives a somewhat pessimistic result in the 1-2 GHz case, as most of the points lie below the line representing the PL-model.

To summarize, a relatively high rate can, in theory, be achieved all the way down to a depth of 16 cm at a relatively low power, especially in the lower frequency ranges, even when taking the large spread in path loss into account. However, it is important to realize that in a practical situation a significant back-off from these bounds must be expected, especially when there is a complexity constraint on the transmitter equipment. We evaluate such scenarios in the next section. It has become clear that one should operate in the lower frequency range in order to keep the power usage at the lowest level. Therefore we will focus on the 1-2 GHz frequency range in the rest of the paper. The problem with this frequency range is that it's a licensed band. We briefly discuss how one may surpass this problem in Section V.

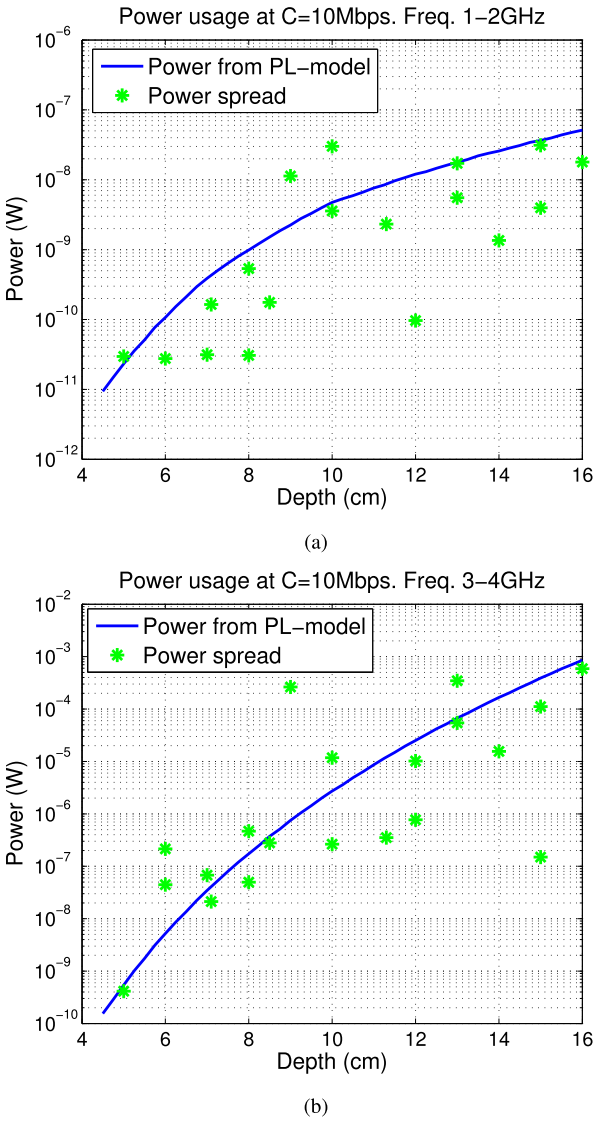


**FIGURE 8.** Spread in necessary transmit power for each measurement point with 10 Mbps capacity constraint. (a) Frequency 1-2 GHz. (b) Frequency 3-4GHz.

## IV. MODULATION

In this section we investigate the minimum transmission power needed for a given rate constraint for implementable modulation- and coding schemes and compare it to the absolute minimum power found in Section III-C. *Pulse Position Modulation* (PPM), binary *Phase Shift Keying* (PSK), and on-off keying are some of the most widely used modulation schemes for UWB, and they are all pulse-based.

Fig. 9 shows the capacity in bits per symbol as a function the channel SNR for PPM- and M-ary PSK modulated inputs with capacity achieving channel codes, i.e., codes with *bit error rate* (BER) $\rightarrow$ 0, for the PL-model derived in Section III-A (these graphs are obtained using Equations (12), (13), (17) and (19) that will be presented in Section IV-B). This is the capacity obtained with modulated channel input. With the exception of 4-PSK (QPSK), MPSK is clearly less power efficient than PPM, and this is the reason why MPSK is not considered in situations where low power consumption is crucial. QPSK, on the other hand, is slightly more power efficient than 2-bit PPM. Since we operate at very low spectral efficiency it is not straight forward to conclude which scheme is the most efficient when both rate and bandwidth are fixed. We therefore evaluate both PPM and QSPK in order to determine the best scheme for the scenario at hand.

In what follows, we will in most cases assume the setup described in Section II, resulting in the total response in (1). We further assume that the transmitter filter, $H_{Tx}(f)$, has an ideal *brick-wall* response, and we only consider the average channel response provided by the PL-model in Section III-A. That is, no power allocation among frequencies are applied.

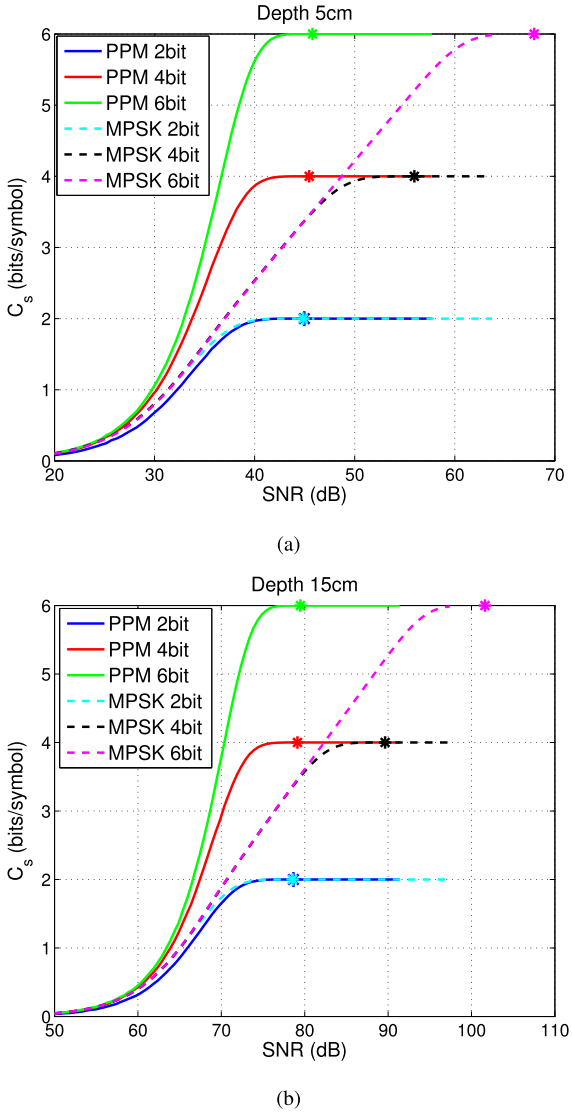


**FIGURE 9.** Capacity for modulated IB-to-OB channel inputs (in bits per symbol) as a function of transmitter power-to-channel noise SNR. The PL model in Section III-A is applied over the frequency band 1-2GHz, with no power allocation, at depths (a) 5cm (b) 15cm. The astrix marks the performance of uncoded modulation for BER = $10^{-6}$.

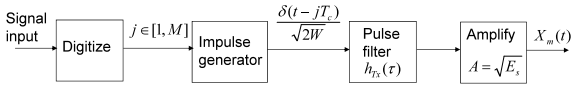


**FIGURE 10.** PPM encoder.

Then, the total channel frequency response becomes

$$H_{\mathrm{Rx}}(f, d) = H_{\mathrm{Tx}}(f)H(f, d), \tag{9}$$

with $H(f, d)$ as defined in (8).

### A. BRIEF DESCRIPTION OF PPM AND QPSK

A block diagram for the PPM encoder is depicted in Fig. 10. The quantized amplitudes of the input signal, represented by indices $j \in [1, M]$, determine the positions of pulses in time. Given that level no. $j$ was produced, an impulse is generated at the time instant $t_0 = jT_c \in [0, T_s]$, where $T_s$ is the symbol time. This impulse is passed through a filter yielding a convenient pulse-shape, $h_{Tx}(t)$, with unit energy, whose width, $T_c$ (referred to as *chip time*), is determined by the available channel bandwidth $W = f_h - f_l$. That is, $T_c = 1/(2\,W)$. With $b$ bits coded into each pulse position, $M = 2^b$ pulse positions are needed in total. Therefore, (unipolar) PPM requires a symbol time of at least $T_s = MT_c$ seconds. The output from the pulse filter is amplified by a factor $\sqrt{E_s}$, where $E_s$ is the symbol energy. Therefore, the PPM modulated output is

$$X_j(t) = \sqrt{E_s} \cdot h_{Tx}(t - jT_c), \tag{10}$$

where, $h_{Tx}$ should be chosen so that it is zero for all $iT_c$, $i \neq j$. At the decoder a *Matched Filter* (MF) receiver is applied to maximize the signal amplitude at the correct time instant. The reader may consult as standard text book like [23, pp. 364-373] for more details.

For frequency selective channels, like the IB-to-OB channel considered here, several versions of the same pulse may appear at different time instants (so-called echoes) making it more difficult to determine the correct pulse time. However, since the channel is slowly varying one may avoid this problem through echo cancellation, or by applying a MF that is matched to both the transmitter pulse and the relevant channel response. Since the goal is to estimate the necessary transmission power in this paper, the latter approach is taken.

We assume that the basics behind QPSK, which is to map the relevant messages onto 4 equidistant discrete points lying on a circle in 2D Euclidean space, is known. The reader may consult for example [23, Ch. 8] for more details. One example on how to implement QPSK for wideband applications can be found in [24].

### B. CAPACITY AND MINIMUM TRANSMISSION POWER WITH MODULATED CHANNEL INPUT

Here we consider the channel capacity obtained with PPM- or QPSK modulated input. That is, the capacity of the Ib-to-OB channel with capacity achieving channel codes (BER$\rightarrow$ 0) followed by discrete modulation at the input. As noted in [25] and [26], the well-known Shannon formula for capacity of an AWGN channel does not apply with discrete modulation schemes at the channel input. The capacity of a PPM- and QPSK modulated channel input was determined in [25] and [27], respectively.

We provide some details for PPM: Let a b-bit sequence, denoted by the vector $\mathbf{U} = [u_1, \cdots, u_b]$, be mapped to a $M = 2^b$ PPM signal $\mathbf{X} = [x_1, \cdots, x_M]$. Each bit-combination is mapped to one (unique) pulse position as the M-dimensional vector $\mathbf{x}_j = [0, 0, \cdots, \sqrt{E_s}, \ldots, 0]^T$ with $\sqrt{E_s}$ placed at the j'th index (see Section IV-A). With $\mathbf{Y}$ the output of the PPM-modulated AWGN channel, one can calculate the capacity as [25].

$$C_s = \max_{P_{\mathbf{X}}(\mathbf{X})} I(\mathbf{Y}; \mathbf{X}). \tag{11}$$

It was shown in [25] that $I(\mathbf{Y};\mathbf{X})$ is maximized whenever $P_{\mathbf{X}}(\mathbf{X})$ is a multivariate uniform distribution, i.e., when each $\mathbf{x}_j$ is equally likely. Let $\mathbf{v}$ be a vector with components $v_j = y_j/\sigma_n$, where $\sigma_n(=\sqrt{N_0\,W})$ is the channel noise standard deviation. The variables $v_j$ are conditionally independent given $\mathbf{x}_1$ and distributed as $v_1 \sim \mathcal{N}(\sqrt{\kappa_s}, 1)$ and $v_j \sim \mathcal{N}(0, 1)$, $j \neq 1$, where $\kappa_s = 2\,E_s/N_0$.[4] It was shown in [25] that the capacity (in bits per symbol) in (11) with PPM modulated input is given by

$$C_{s(PPM)}(\kappa_s) = \log_2(M) - E_{\mathbf{v}|\mathbf{x}_1}\left\{\log_2\left(\sum_{j=1}^{M} e^{\sqrt{\kappa_s}(v_j - v_1)}\right)\right\}, \tag{12}$$

where $E_{\mathbf{v}|\mathbf{x}_1}$ is the expectation w.r.t. the conditional pdf $p(\mathbf{v}|\mathbf{x}_1)$. One can evaluate the M-fold integral constituting the expectation operation $E_{\mathbf{v}|\mathbf{x}_1}$ in (12) by Monte Carlo integration as illustrated in Appendix.

For an MPSK modulated input, one can under similar assumptions as for PPM calculate the capacity (in bits per channel use) as [27]

$$C_{s(MPSK)} = \log_2(M) - E_w\left\{\log_2\left(\sum_{k=1}^{M} e^{-\frac{|a_1+w-a_k|^2-|w|^2}{2\sigma_n^2}}\right)\right\}, \tag{13}$$

where $w$ is a complex white Gaussian noise process and $a_k = \sqrt{P_s}\,e^{ik2\pi/M}$ are complex numbers (lying on a circle) defining the modulation constellation. $P_s$ is the (2-dimensional) symbol power. The expectation, $E_w\{\cdot\}$, in (13) can by evaluated by Monte Carlo integration in a similar way as that shown in Appendix for PPM. The performance of QPSK is obtained by setting $M = 4$.

Note that the *signal-to-noise ratio* (SNR) is defined as $\beta = |a_k|^2/(2\sigma_n^2)$, with $\sigma_n^2 = N_0\,W$, and is related to $\kappa_s$ in (12) as $\kappa_s = 2\beta$.

The capacity in bits per second (bps) is found by dividing $C_s$ by the symbol time $T_s$

$$C_b = \frac{C_s}{T_s} = \frac{C_s}{MT_c} = \frac{2C_sW}{M}, \tag{14}$$

where the last two equalities are valid for a PPM modulated input (or any other orthogonal modulation scheme). For MPSK (and QPSK) one can simply put $M = 4$.

For PPM the maximal bit-rate per second for a given $M$ is therefore $2\,W\log_2(M)/M$. If the bandwidth, $W$, is finite, there will be a certain $M$ above which PPM cannot provide a given bit-rate. Therefore, for a fixed (finite) $W$, there is a tradeoff between the number of pulse positions $M$ (lowering the transmission power) and the maximal bit rate $C_b$ that can be obtained. Therefore, to obtain a certain required rate for fixed bandwidth, one cannot limit the power beyond a certain minimum. The maximal rate for QPSK, on the other hand, is $\log_2(4)W/2 = W$.

[4]With a uniform input distribution one can choose conditioning on any $\mathbf{x}_n$, $n \neq j$ due to symmetry. Here $n = 1$ is chosen.

In the following we compare three cases: 1) A fixed bandwith of $W = 1$ GHz with no power allocation. 2) Signalling within the $\rho = 0.5$ CBW (see Section III-B). 3) A fixed bandwith of $W = 1$ GHz with optimal power allocation.

When no power allocation is assumed, the relation between the received- and transmitted power is given by (3), with $H_{\mathrm{Rx}}(f, d)$ as defined in (9). With optimal power allocation, the relation between transmitted and received power is found from

$$P_{Rx} = \int_{f_l}^{f_h} P^*(f)|H(f, d)|^2 \mathrm{d}f, \tag{15}$$

where the transmitted power, $P_{Tx}$, is given by (7), $P^*(f)$ is given by (6) and the measured average channel response, $H(f, d)$, is given by (8).

The power needed to obtain a certain capacity is determined by $\kappa_s$ (or $\beta$) and is found by numerically solving $C_s$ in (12) (or (13)) w.r.t. $\kappa_s$ (or $\beta$). Once this value is found we can determine the necessary transmit power, in the absence of power allocation, by dividing with $\gamma(d)$ in (3) with $H_{\mathrm{Rx}}$ given in (9). We will further need the below relationship (see [28]),

$$\left(\frac{E_b}{N_0}\right)_{\min} = \frac{1}{C_b}\frac{P}{N_0} = \frac{1}{C_b}\beta = \frac{\kappa_s}{2C_b}, \tag{16}$$

where $E_b$ is the energy per bit, $P$ is the average power, and $(E_b/N_0)_{\min}$ denotes the minimum obtainable $E_b/N_0$. Since the average power is given by $P = E_s/T_s$ then, for PPM, $P = E_s/(MT_c) = 2\,E_sW/M$. With the relationship in (16), the definition of $\kappa_s$, and the noise power for bandwidth $W$, $N_0\,W$, it follows that the transmission power is

$$P_{Tx(PPM)} = \frac{N_0W\kappa_s}{M\gamma(d)}. \tag{17}$$

The subscript '$Tx$' refers to transmitted power/energy. The average energy per bit is found from

$$E_{b_{Tx(PPM)}} = \frac{P_{Tx(PPM)}}{C_{b(PPM)}} = \frac{N_0W\kappa_s}{MC_{b(PPM)}\gamma(d)} = \frac{N_0\kappa_s}{2C_{s(PPM)}\gamma(d)}. \tag{18}$$

Similarly, for QPSK, we have

$$P_{Tx(QPSK)} = \frac{N_0W\beta}{2\gamma(d)} \tag{19}$$

and the average energy per bit is found from

$$E_{b_{Tx(QPSK)}} = \frac{P_{s_{Tx(QPSK)}}}{C_{b(QPSK)}} = \frac{N_0W\beta}{2C_{b(QPSK)}\gamma(d)} = \frac{N_0\beta}{C_{s(QPSK)}\gamma(d)}. \tag{20}$$

To determine the necessary transmission power for a target rate, $C_b$, bandwidth, $W$, and cardinality $M$, one can use (17) (or (19)). Given $N_0$ for room temperature, $\kappa_s$ (or $\beta$) is found

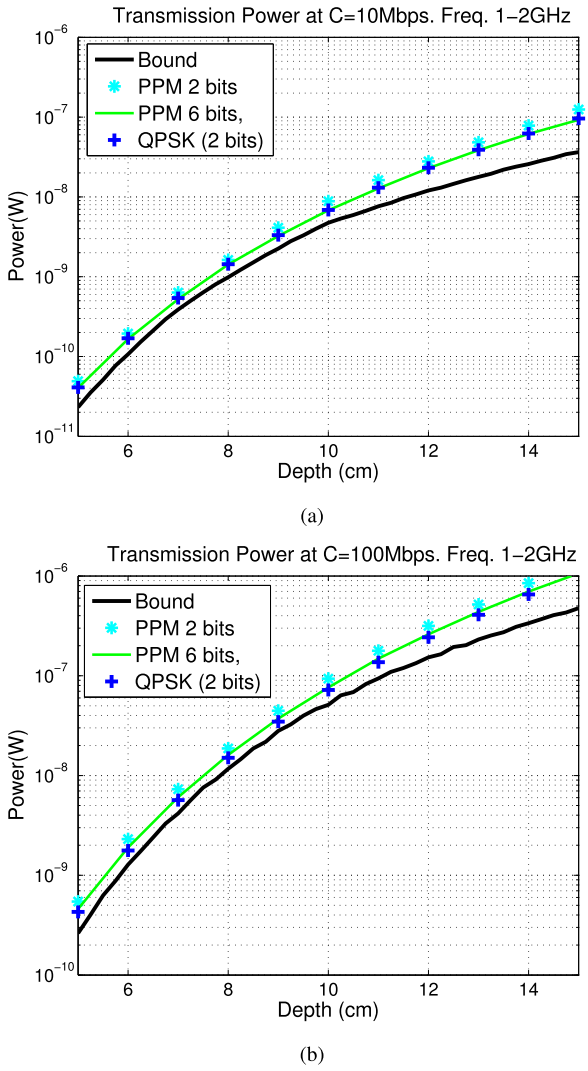


**FIGURE 11.** Necessary transmission power for PPM and QPSK to obtain a capacity constraint of (a) 10Mbps (b) 100Mbps.

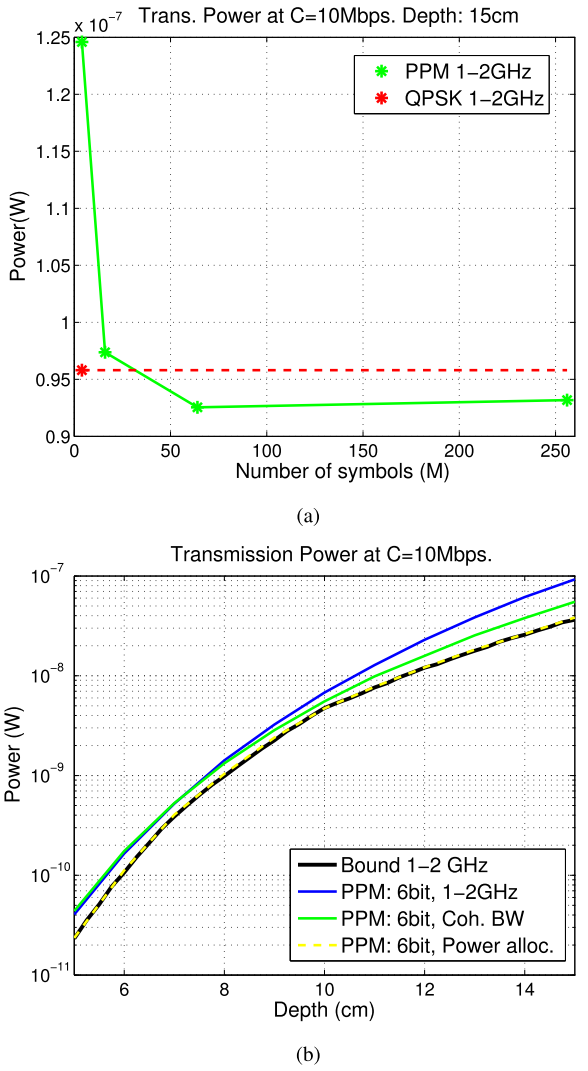


**FIGURE 12.** (a) Necessary transmission power needed for PPM to achieve 10 Mbps rate constraint as a function of the number of symbols $M$ for the frequency band 1-2 GHz. (b) Example showing gain in lowered transmission power for PPM using ($\rho = 0.5$) CBW in 1-2 GHz band and the loss compared to optimal power allocation for 10 Mbps capacity constraint.

by solving (12) (or (13)) for the given rate $C_s$, with respect to $\kappa_s$ (or $\beta$).

Fig. 11 shows the necessary transmission power for the frequency band 1-2 GHz for capacity constraints of $C_b = 10$ Mbps and 100 Mbps, as a function of depth.

Although PPM is known to be power efficient, QPSK is very close to (even slightly better at 100Mbps) 6-bit ($M = 64$) PPM for the rate and bandwidth considered. The two most probable reasons are: i) With $C_b = 10^7$ and $10^8$ bps and with $W = 1$ GHz we have a very low spectral efficiency where both PPM and QPSK have nearly the same performance (see Fig. 9 at the lowest SNR). ii) QPSK can send more symbols (pulses) per second than PPM which needs $MT_c$ time slots for each symbol (pulse). However, as $M$ gets large enough, QPSK will become inferior to PPM. This is illustrated in Fig. 12(a) for $C_b = 10^7$ bps, where QPSK becomes inferior to QPSK As $M > 2^5$. However, by increasing $M$ beyond $2^6$, no further lowering of transmission power is observe as a larger bandwidth would be necessary. Therefore the gain over QPSK for this specific channel is rather minute.

An alternative is to send only within the CBW. Fig. 12 shows the performance of PPM when using the $\rho = 0.5$ CBW (from Fig. 5) compared to the whole $1-2$ GHz band both with and without optimal power allocation, all for 6 bits per pulse. There is a clear loss from the optimal power allocation case which is nearly operating at the (AWGN) capacity bound. Power allocation over the frequency band 1-3 GHz was also tested, but led to no gain over the 1-2 GHz band. This implies that increasing the frequency band beyond 1 GHz does not help in lowering the transmit power any further. Also, in the absence of power allocation, less power is required at larger depths when only the CBW is applied compared to the whole $1-2$ GHz band. This can be understood from the *waterfilling*

*principle* since power is wasted on bands with too much attenuation.

One can also observe from Fig. 12(a) that the performance does not improve much beyond $M = 64$ symbols per time slot (this may be why 6-bit PPM nearly achieves the capacity bound when optimal power allocation is performed in Fig. 12(b)). Increasing the encoder complexity in order to obtain an $M > 64$ is therefore of little interest for the rates and bandwidths considered.

The procedure presented in this section may be followed for other capacity constraints and channel models to determine the bandwidth $W$ and cardinality $M$.

### C. UNCODED- AND REED-SOLOMON CODED MODULATION

From a practical perspective it is of interest to evaluate how an uncoded system, or a system with an implementable channel code, performs for a given target *bit error rate* (BER). This gives an idea of the transmission power level requirement for a practical system.

First we need a relation between the BER, denoted $Pr_b$, and the symbol error probability, $Pr_s$. If all symbol errors are equally likely, which is the case when we have the same spacing between all neighboring vectors in the modulation constellations as well as uniform distribution over the input alphabet, then [23, p.500]

$$Pr_s = \frac{2Pr_b(M-1)}{M}. \tag{21}$$

For uncoded PPM modulation, the symbol error probability is given by [25, p.20]:

$$Pr_{s(PPM)} = 1 - \frac{1}{\sqrt{2\pi}} \int_{-\infty}^{\infty} e^{-\frac{(v-\sqrt{\kappa_s})^2}{2}} \Phi(v)^{M-1} \mathrm{d}v, \tag{22}$$

where

$$\begin{aligned}\Phi(v) &= \frac{1}{\sqrt{2\pi}} \int_{-\infty}^{v} e^{-\frac{u^2}{2}} \mathrm{d}u = \frac{1}{2\sqrt{2}} \frac{2}{\sqrt{\pi}} \int_{-\infty}^{v} e^{-\frac{u^2}{2}} \mathrm{d}u \\ &= \frac{1}{2\sqrt{2}} \mathrm{erf}\left(\frac{v}{\sqrt{2}}\right),\end{aligned} \tag{23}$$

and erf(·) is the *error function* [23, p. 806]. For uncoded QPSK the symbol error probability is given by [23, p. 547]

$$Pr_{s(QPSK)} = 1 - \mathrm{erf}\left(\sqrt{\beta} \sin\left(\frac{\pi}{4}\right)\right). \tag{24}$$

The necessary bit energy is then

$$\begin{aligned}E_{b(PPM)} &= \frac{N_0 W \kappa_s}{M R_{b(PPM)} \gamma(d)}, \\ E_{b(QPSK)} &= \frac{N_0 W \beta}{2 R_{b(QPSK)} \gamma(d)},\end{aligned} \tag{25}$$

where $R_{b(PPM)} = 2\,W \log_2(M)/M$ [23, p. 656] and $R_{b(QPSK)} = W$ [23, p. 655]. The necessary transmission power is again given by (17) and (19).

Ideally one should compare the necessary transmission power of uncoded PPM and QPSK for a given BER- and rate constraint for the relevant channel bandwidth. However, since the obtainable rate with bandwidth $W$ at a given BER varies significantly with the modulation schemes as well as with the cardinality $M$, such a comparison is impossible. However, when channel coding is applied prior to modulation one can, by choosing the appropriate "code rate", make each coded modulation scheme communicate at the same information rate. The processing power will increase somewhat, but one will also achieve a "coding gain" resulting in lowered transmission power for a target BER.

We will consider *Reed-Solomon (RS) codes* [14] mainly for two reasons: First, since these codes operate on symbols instead of bits, they are well suited for M-ary modulation schemes. Secondly, RS-codes are efficient at correcting *error bursts* which typically emerge when shadowing is present on the channel medium as well as when PPM modulation is applied (a PPM symbol may be confused with any other symbol with equal likelihood if the channel SNR drops below the optimal operation point [13, p. 627]).

Typically an $(N, K)$ RS code outputs blocks of $N = 2^m - 1$ "code symbols", where $m$ is the number of bits per coded symbol. Then $K$, the block size of message symbols (also of b bits each) at the input of the RS coder, can be chosen so that a specific *code rate*, $r_c = K/N$, is obtained. RS codes exist for any $0 < K < N < 2^m + 2$, it has the largest possible minimum (codeword) distance among any liner code, $d_{min} = N - K + 1$, and can correct up to $(N-K)/2$ symbol errors [29, pp. 237-240]. The codeword is basically a concatenation of $K$ message symbols and $N - M$ *parity symbols* which are the remainder of a polynomial division between the *message polynomial* and the RS codes' *generator polynomial* [29, pp. 238-239]. The encoder consists of $N - K$ $m$-bit multiplicators, modulo-$m$ adders and $m$-bit storage devices, and is depicted in [29, p. 239]. Such codes should be possible to implement in a typical WCE, at least with the number of parity symbols considered in this paper. Note also that RS codes have their optimal performance around a code rate of $r_c = 3/4$, but does not deviate significantly from this optimal value between $0.5 < r_c < 0.9$. This is nicely illustrated in [25, p. 25].

With $M$-ary modulation applied on the RS encoder output, the simplest choice is to match the modulation alphabet with the RS codes alphabet. That is, choose $M = 2^m$. However, it is possible to map between arbitrary alphabets using the method in [30]. A method for soft-decoding of RS codes was given in [31]. This may be applied to enhance the system performance without placing any further computational load on the encoder side. Here we will assume that the code- and modulation alphabets are the same, i.e. $m = b$ and so each code symbol is mapped directly onto one of the $M = 2^b$ modulation symbols, as well as hard decision at the receiver side. Then

$$Pr_c = \frac{1}{N} \sum_{j=1+(N-K)/2} j \binom{N}{j} Pr_s^j (1 - Pr_s)^{N-j}, \tag{26}$$

serves as the upper bound on the decoding error probability, where $Pr_s$ is as in (22) (PPM) or (24) (QPSK).

Given a rate constraint, $R_{min}$, a BER requirement, $Pr_b$, and a certain bandwidth, $W$, one can determine the necessary transmission energy and power as follows: 1) Given $M$, determine $N$ and $K$ so that we are close to $R_{min}$, then compute $Pr_c$ from (21). Here we choose $N = M - 1$, which is common for RS codes. 2) With $N$, $K$ and $Pr_c$ determined, one can find $Pr_s$ from (26). $\kappa_s$ or SNR can then be found from (22) or (24) respectively. 3) Use the formulas in (25) to compute the necessary energy per bit, where now $R_{b(PPM)} = 2\,Wr_c \log_2(M)/M$ and $R_{b(QPSK)} = Wr_c$ The transmission power is then given by (17) and (19).

*Examples:* We compare the necessary transmission power for information rate $R \approx 100$ Mbps and BER $Pr_b = 10^{-6}$ for the following examples:

**i:** 5-bit PPM with capacity achieving codes, or *optimal* 5-bit PPM, using the $\rho = 0.5$ CBW.

**ii:** Uncoded 7-bit PPM with $W = 1$ GHz, with and without power allocation.

**iii:** RS-coded 5-bit PPM where RS codes are tailored to the $\rho = 0.5$ CBW at each depth.

**iv:** RS(31,25) coded 5-bit PPM and $W = 0.41$ GHz, corresponding to the $\rho = 0.5$ CBW at 16 cm depth.

**v:** RS(31,27) coded 5-bit PPM and $W = 0.36$ GHz, corresponding to the $\rho = 0.6$ CBW at 16 cm depth.

**vi:** RS(15,11) coded 4-bit PPM and $W = 0.27$ GHz, corresponding to the $\rho = 0.7$ CBW at 14 cm depth.

**vii:** RS(15,7) coded QPSK and $W = 0.22$ GHz, corresponding to the $\rho = 0.7$ CBW at 16 cm depth.

Note that for all these examples the rate, $R_b$, may vary within $\pm 10$ Mbps. For the example vii) we chose a RS(15,7) code and communicate one codeword over 2 QPSK transmissions instead of using a $N = 3$-based code on one transmission, which will enhance the error correcting abilities. The error probability$\tilde{Pr}_s$ now includes two events, each with probability $Pr_s$ (as in in (24)), and follows from the rules of probability for two events (one for each transmission), i.e., $\tilde{Pr}_s = 2\,Pr_s - Pr_s^2$.

Fig. 13 shows the performance of all the above listed examples.

From Fig. 13(a) one can notice several things. Naturally, there is a significant gap between the system with capacity achieving channel codes (example i, green curve) and the RS-coded/uncoded ones. One can see from the two uncoded examples (example ii, red and yellow curves) that power allocation helps, most so at larger depths. However, both of these uncoded 7-bit systems are clearly outperformed by RS coded 5-bit PPM (examples iii/iv, cyan dashed/blue curves) at larger depths (below 7 cm). It may therefore be beneficial to choose a modulation scheme with lower cardinality and then apply channel coding. Another thing to notice is that the gain obtained by choosing the CBW for each depth and adapting the RS code correspondingly (example iii, depicted by the cyan dashed curve), only brings a gain over a fixed bandwidth $W = 0.41$ GHz and a fixed RS

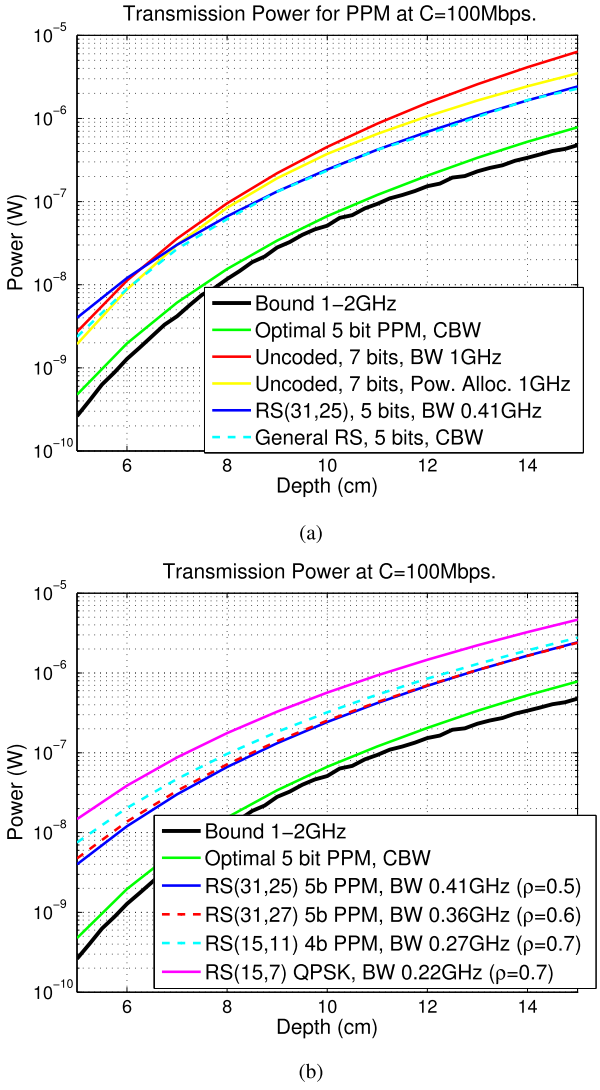


**FIGURE 13.** Examples on necessary transmission power when $R_b \approx 100$ Mbps and $Pr_b = 10^{-6}$. (a) RS-coded and uncoded PPM. (b) RS-coded PPM and QPSK.

code chosen for that bandwidth (case iv depicted by the blue curve), for depths smaller than $7 - 8$ cm. Since it is the larger depths that are the most critical with respect to power usage, one may therefore choose the code and bandwidth which works best at larger depths without losing a lot at more shallow depths. This strategy will lower encoder complexity.

The blue and dashed red curves in Fig. 13(b) show the necessary power (for all relevant depths) when the CBW at 16 cm depth is applied for increasing values of $\rho$ (i.e., examples iv and v). It is clear that increasing $\rho$ beyond 0.5 does not help, since a decline in performance is observed. However, the RS(31,25) code is closest to the optimal operation of $r_c = 3/4$, and it can correct more errors than the (31,27) code, which may be a reason why the result declines. The RS(15,11) coded 4-bit PPM scheme (example vi, cyan dashed curve) performs rather well given that its cardinality is lower. The same can be said about the QPSK system (example vii,

magenta curve) which has the lowest cardinality among all the examples.

Note that QPSK with capacity achieving channel codes was performing close to 6-bit PPM with capacity achieving channel codes as seen in Fig. 11(b). The reason for the discrepancy between these cases may be: 1) We operate at a higher number of bits per channel symbol than in Section IV-B. I.e., $R_s = 1$ (QPSK) and $R_s = 4$ (PPM) versus $C_s = 0.20$ in Section IV-B (for both systems). The difference between these situations can be seen in Fig. 9. 2) RS codes with hard decision are optimal around $r_c \approx 3/4$ [25, p.25], whereas the RS(15,7) code used with QPSK has code rate of $r_c \approx 0.5$.

## V. SUMMARY AND CONCLUSIONS

In this paper the necessary transmission power needed obtain a certain target data rate for in-body to on-body communication, considering a measurement based UWB channel model in the 1-6 GHz range, has been investigated. The necessary power is analyzed for three scenarios: i) Channel capacity (minimum power bound). ii) Capacity with PPM and QPSK modulated input. iii) PPM and QPSK modulation with Reed-Solomon (RS) channel coding. The available bandwidth as well as the corresponding modulation cardinality has been investigated. The main findings are listed below:

1) Huge savings in transmission power is obtained by operating in the lower frequency ranges (1-2 GHz) due to the significant increase of channel attenuation with (increasing) frequency. Even when a bandwidth of 3 GHz is applied over the $3-6$ GHz band one needs in the order of $2 \cdot 10^4$ times more transmission power compared to applying 1GHz bandwidth in the 1-2 GHz band for the same rate constraint. Since the transmitter antennas used during the channel measurements were not optimal in the 1-2GHz range, this estimate may even be conservative.

2) The capacity for a given transmit power constraint does not increase, and the necessary transmit power for a given capacity constraint does not decrease when using a bandwidth larger than 1GHz, even with optimal power allocation assuming perfect knowledge of the channels characteristics. This is in line with the investigation in [8]. At larger depths the useful bandwidth may be significantly smaller.

3) With capacity achieving codes, the performance of PPM for a given cardinality, $M$, and QPSK does not differ significantly. This is due to the low spectral efficiency typical for UWB communication. That is, one cannot fully utilize the large gains possible with PPM with a large cardinality ($M$), since the useful bandwidth is too small (below 1 GHz): Increasing $M$ beyond $2^6$ leads to negligible improvements. Also, in line with this, when optimal power allocation is applied, PPM operate nearly at the capacity bound when $M = 2^6$.

4) Not surprisingly, a backoff from modulation with capacity archiving codes is observed for uncoded modulation and modulation with RS-codes. That is, a 5-10 times increase in transmission power is needed. There is now a more significant benefit of using PPM in terms of lowered transmission power (as seen in Fig. 9). The best performance for a given cardinality ($M$) is obtained by choosing different RS codes with code-rate tailored to the coherence bandwidth (CBW) at a given depth. However, by using the CBW provided by the relevant path loss model at the largest depth (16 cm), which is approximately 0.4 GHz, then choosing the best RS code for this case, one does quite well at all depths. The small loss compared to the case where both CBW and RS codes are tailored to each depth is only observed at shallower depths than 7-8 cm.

One important conclusion is that if large gains are to be obtained over narrowband alternatives, like the MICS band, it would be advantageous to communicate in the $1-2$ GHz range (see Fig. 7(b)). Although the 1-2 GHz band is a licensed band, it may be applicable in certain closed environments if proper measures are taken. Since WCE screening will likely take place in a hospital environment, or at home, and given the fact that the radiation will be quite small due to the large attenuation in the human body, one could use the licensed band under proper shielding. For example, one may use a vest that limits the radiation leaking into the surrounding environment to an acceptably low level, as well as preventing radiation from external equipment interfering with the communication.

Moving even further down in frequency would likely be even more power saving. However, an increase in the size of the transmitter antenna would then be necessary. For future investigations, it would be advantageous to perform experiments using transmitter antennas optimized for the 1-2 GHz range.

## APPENDIX
## PPM CAPACITY BY MONTE CARLO INTEGRATION

Draw $n$ trials of $\mathbf{v}$ following $p(\mathbf{v}|\mathbf{x}_1)$. For each trial calculate $\log_2(1 + (M-1)e^{\kappa_s/2}e^{-\sqrt{\kappa_s}v_1})$. Then (assuming ergodicity), the expectation in (12) can be approximated by [32, p. 285]

$$\frac{1}{n}\sum_{n} \log_2\left(1 + (M-1)e^{\kappa_s/2}e^{-\sqrt{\kappa_s}v_1}\right)_n, \tag{27}$$

with equality as $n \to \infty$. Since all components of $\mathbf{v}$ are independent, drawing $\mathbf{v}$ according to $p(\mathbf{v}|\mathbf{x}_1)$ is equivalent to drawing $v_1 \sim \mathcal{N}(\sqrt{\kappa_s}, 1)$ and $v_i \sim \mathcal{N}(0, 1)$, $i = 2, \cdots, M$ [25, p. 10].

## REFERENCES

[1] A. M. D. Wolf, "Colorectal cancer screening for average-risk adults: 2018 guideline update from the american cancer society," *CA, Cancer J. Clinicians*, vol. 68, no. 4, pp. 250–281, Jul/Aug. 2018. [Online]. Available: https://onlinelibrary.wiley.com/doi/abs/10.3322/caac.21457
[2] A. Wang *et al*, "Wireless capsule endoscopy," *Gastrointestinal Endoscopy*, vol. 78, no. 6, pp. 805–815, 2013.
[3] P. Swain, "The future of wireless capsule endoscopy," *World J. Gastroenterol.*, vol. 14, no. 26, pp. 4142–4145, Jul. 2008.
[4] T. M. Cover and J. A. Thomas, *Elements of Information Theory*. New York, NY, USA: Wiley, 2006.
[5] R. Chavez-Santiago and I. Balasingham, "Ultrawideband signals in medicine [life sciences]," *IEEE Signal Process. Mag.*, vol. 31, no. 6, pp. 130–136, Nov. 2014.
[6] *IEEE Standard for Local and Metropolitan Area Networks—Part 15.6. Wireless Body Area Networks*. IEEE Standard 802.15.6-2012, 2012.

[7] J.-C. Brumm and G. Bauch, "On the placement of on-body antennas for ultra wideband capsule endoscopy," *IEEE Access*, vol. 5, pp. 10141–10149, 2017.

[8] J.-C. Brumm and G. Bauch, "Channel capacity and optimum transmission bandwidth of in-body ultra wideband communication links," in *Proc. 11th Int. ITG Conf. Syst. Commun. Coding*, Hamburg, Germany, Feb. 2017, pp. 1–6.

[9] J. Shi, D. Anzai, and J. Wang, "Channel modeling and performance analysis of diversity reception for implant UWB wireless link," *IEICE Trans. Commun.*, vol. E95-B, no. 10, pp. 3197–3205, Oct. 2012.

[10] Y. Shimizu, D. Anzai, R. Chavez-Santiago, P. A. Floor, I. Balasingham, and J. Wang, "Performance evaluation of an ultra-wideband transmit diversity in a living animal experiment," *IEEE Trans. Microw. Theory Techn.*, vol. 65, no. 7, pp. 2596–2606, Jul. 2017.

[11] K. Katsu, D. Anzai, and J. Wang, "Performance evaluation on correlation detection and energy detection for ultra wideband-impulse radio communication with multi-pulse position modulation scheme in implant body area networks," *IET Commun.*, vol. 7, no. 13, pp. 1430–1436, Sep. 2013.

[12] P. A. Floor *et al.*, "In-body to on-body ultrawideband propagation model derived from measurements in living animals," *IEEE J. Biomed. Health Inform.*, vol. 19, no. 3, pp. 938–948, May 2015.

[13] J. M. Wozencraft and I. M. Jacobs, *Principles of Communication Engineering*. New York, NY, USA: Wiley, 1965.

[14] I. S. Reed and G. Solomon, "Polynomial codes over certain finite fields," *J. Soc. Ind. Appl. Math.*, vol. 8, no. 2, pp. 300–304, 1960.

[15] S. Aoyama, D. Anzai, and J. Wang, "SAR evaluation based on required BER performance for 400 MHz implant BANs," in *Proc. Asia–Pacific Symp. Electromagn. Compat.*. Singapore, May 2012, pp. 365–368.

[16] H. T. Friis, "A note on a simple transmission formula," *Proc. IRE*, vol. 34, no. 5, pp. 254–256, May 1946.

[17] A. N. Kim, P. A. Floor, T. A. Ramstad, and I. Balasingham, "Communication using ultra wide-band pulse position modulation for in-body sensors," in *Proc. 7th Int. Conf. Body Area Netw.*, Oslo, Norway, 2012, pp. 159–165.

[18] T. Sereewattanapong and S. Promwong, "Evaluation of ultra wideband impulse radio transmission loss due to laptop computer," in *Proc. IEEE 9th Int. Conf. Commun. (MICC)*, Kuala Lumpur, Malaysia, Dec. 2009, pp. 259–262.

[19] Q. Wang, K. Wolf, and D. Plettemeier, "An UWB capsule endoscope antenna design for biomedical communications," in *Proc. 3rd Int. Symp. Appl. Sci. Biomed. Commun. Technol. (ISABEL)*, Rome, Italy, Nov. 2010, pp. 1–6.

[20] S. Brovoll, O. Aardal, T. Paichard, T. Berger, T. R. Lande, and S.-E. Hamran, "Optimal frequency range for medical radar measurements of human heartbeats using body-contact radar," in *Proc. 35th Annu. Int. Conf. IEEE Eng. Med. Biol. Soc. (EMBC)*, Osaka, Japan, Jul. 2013, pp. 1752–1755.

[21] J. D. Parsons, *The Mobile Radio Propagation Channel*. 2nd ed. Hoboken, NJ, USA: Wiley, 2000.

[22] D. Tse and P. Viswanath, *Fundamentals of Wireless Communication*. Cambridge, U.K.: Cambridge Univ. Press, 2005.

[23] S. Haykin, *Communications System*, 3rd ed. Hoboken, NJ, USA: Wiley, 1994.

[24] S. Kang, S. V. Thyagarajan, and A. M. Niknejad, "A 240GHz wideband QPSK transmitter in 65nm CMOS," in *Proc. IEEE Radio Freq. Integr. Circuits Symp.*, Tampa FL, USA, Jun. 2014, pp. 353–356.

[25] A. Dolinar, D. Divsalar, J. Hamkins, and F. Pollara, "Capacity of pulse-position modulation (PPM) on Gaussian and Webb channels," Jet Propuls. Lab., California Inst. Technol., California, CA, USA, TMO Progress Rep., Aug. 2000.

[26] S. Dolinar, D. Divsalar, J. Hamkins, and F. Pollara, "Capacity of PPM on Gaussian and Webb channels," in *Proc. IEEE Int. Symp. Inf. Theory*, Sorrento, Italy, Jun. 2000, p. 410.

[27] G. Ungerboeck, "Channel coding with multilevel/phase signals," *IEEE Trans. Inf. Theory*, vol. IT-28, no. 1, pp. 55–67, Jan. 1982.

[28] S. Verdu, "Spectral efficiency in the wideband regime," *IEEE Trans. Inf. Theory*, vol. 48, no. 6, pp. 1319–1343, Jun. 2002.

[29] S. Lin and D. J. Costello, Jr., *Error Control Coding*, 2nd ed. Upper Saddle River, NJ, USA: Pearson Prentice Hall, 2004.

[30] K.-P. Yar, D.-S. Yoo, and W. Stark, "Performance of RS coded M-ary modulation with and without symbol overlapping," *IEEE Trans. Commun.*, vol. 56, no. 3, pp. 445–453, Mar. 2008.

[31] R. Koetter and A. Vardy, "Algebraic soft-decision decoding of Reed-Solomon codes," *IEEE Trans. Inf. Theory*, vol. 49, no. 11, pp. 2809–2825, Nov. 2003.

[32] A. Papoulis and S. U. Pillai, *Probability, Random Variables, and Stochastic Processes*, 4th ed. New York, NY, USA: McGraw-Hill, 2002.


**PÅL ANDERS FLOOR** received the B.Sc. degree from Gjøvik University College, Gjøvik, Norway, in 2001, and the M.Sc. and Ph.D. degrees from the Department of Electronics and Telecommunications, Norwegian University of Science and Technology (NTNU), Trondheim, Norway, in 2003 and 2008, respectively, all in electrical engineering. He held a Postdoctoral position with the Intervention Center, Oslo University Hospital, and the Institute of Clinical Medicine, University of Oslo, Oslo, Norway, and the Department of Electronics and Telecommunications, NTNU, from 2008 to 2015. He currently holds a Postdoctoral position with the Norwegian Color and Visual Computing Laboratory, Department of Computer Science, NTNU. His current research interests include joint source-channel coding, information theory and signal processing applied on point-to-point links, in small and large networks, and in neuroscience as well as lightweight cryptography for low complexity devices. He is currently doing research on communication and image enhancement for capsule endoscopy.

**RAÚL CHÁVEZ-SANTIAGO** was born in Oaxaca, Mexico. He received the Ph.D. degree in electrical and computer engineering from the Ben-Gurion University of the Negev, Beersheba, Israel, in 2007. From 2007 to 2008, he held a Postdoctoral position with the University Paris-Sud XI, Paris, France, where he investigated the radio resource management for mobile WiMAX systems. He then became a Postdoctoral Fellow with Bar-Ilan University, Ramat Gan, Israel, researching the information theory aspects of ad hoc and cognitive radio networking. He was with the Intervention Center, Oslo University Hospital, Norway, from 2009 to 2015, where he investigated short-range radio communication technologies for body area networks and implantable biomedical sensors. He currently pursues diverse entrepreneurial opportunities including radio technology for healthcare.

**ANNA N. KIM** received the Dr.Ing. degree from the Department of Electronics and Telecommunications, Norwegian University of Science and Technology (NTNU), Trondheim, Norway, in 2005. Since her graduation, she had been a Postdoctoral Researcher with the Q2S Centre, Centre of Excellence, NTNU, and later on at the Intervention Centre, Oslo University Hospital. In 2012, she joined the SINTEF ICT as a Research Scientist. Since 2017, she has been with Elliptic Labs, where she focuses on research and development of ultrasound-based user interaction using machine learning. Her research interests include image processing and communications, signal processing for wireless sensor networks, resource allocation, source/channel coding, and communication theory.

**KIMMO KANSANEN** received the M.Sc. degree in electrical engineering and Dr.Tech. degree from the University of Oulu, Finland, in 1998 and 2005, respectively. He was a Research Scientist and a Project Manager with the Centre for Wireless Communications, University of Oulu. Since 2006, he has been with the Norwegian University of Science and Technology, Trondheim, Norway, where he has been a Professor, since 2016. His research interests include wireless communications and signal processing. He is an Associate Editor of the IEEE TRANSACTIONS ON WIRELESS COMMUNICATIONS.

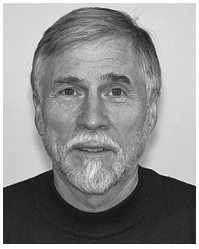

**TOR A. RAMSTAD** was born in Norway. He received the Siv.Ing. and Dr.Ing. degrees from the Norwegian Institute of Technology, in 1968 and 1971, respectively. From 1982 to 1983, he was a Visiting Associate Professor with the University of California at Santa Barbara (UCSB), Santa Barbara. He has held various positions with the Department of Electronic Systems, Norwegian University of Science and Technology, where he has been a Full Professor of telecommunications, since 1983, and has been a Professor Emeritus, since 2014. He was with the Georgia Institute of Technology as a Visiting Adjunct Professor from 1989 to 1990, and with UCSB as a Visiting Professor from 1997 to 1998 and from 2008 to 2009. From 2003 to 2004, he was a Visiting Professor with EURECOM, France. He has published over 270 journals and full conference papers and has supervised over 35 Ph.D. and 300 master students. His research interests include multi-rate signal processing, speech, image, and video communications, with emphasis on joint source-channel coding.

**ILANGKO BALASINGHAM** (SM'12) received the M.Sc. and Ph.D. degrees in signal processing from the Department of Electronics and Telecommunications, Norwegian University of Science and Technology (NTNU), Trondheim, Norway, in 1993 and 1998, respectively. He performed the master's degree thesis with the Department of Electrical and Computer Engineering, University of California at Santa Barbara, Santa Barbara, CA, USA. From 1998 to 2002, he was a Research Engineer developing image and video streaming solutions for mobile handheld devices with the Fast Search and Transfer ASA, Oslo, Norway, which is currently a part of Microsoft Inc. Since 2002, he has been with the Intervention Center, Oslo University Hospital, Oslo, Norway, as a Senior Research Scientist, where he heads the Wireless Sensor Network Research Group. He was appointed as a Professor in signal processing in medical applications with NTNU, in 2006. From 2016 to 2017, he was a Professor by courtesy with the Frontier Institute, Nagoya Institute of Technology, Japan. He has authored or co-authored over 250 journal- and conference papers, seven book chapters, 42 abstracts, five patents, and 16 articles in popular press. His research interests include super robust short range communications for both in-body and on-body sensors, body area sensor networks, microwave short range sensing of vital signs, short range localization and tracking mobile sensors, and nanoscale communication networks. He has given 16 invited/keynotes at the international conferences. In addition, he is active in organizing conferences (Steering Committee Member of ACM NANOCOM, from 2018 to 2021; General Chair: the 2019 IEEE International Symposium of Medical ICT and the 2012 Body Area Networks Conference; and TPC Chair of the 2015 ACM NANOCOM), and Editorial Board [has been an Area Editor of the *Nano Communication Networks* (Elsevier), since 2013].